JOURNAL OF MATERIALS SCIENCE **39** (2004) 4855–4860

Dopant-dependent oxidation behavior of α-SiAlON ceramics

JAY YU, HENRY DU
Department of Chemical, Biomedical and Material Engineering, Stevens Institute of Technology, Hoboken, NJ 07030, USA

ROMAN SHUBA, I-WEI CHEN
Department of Materials Science and Engineering, University of Pennsylvania, Philadelphia, PA 19104, USA

Oxidation behavior of α-SiAlON ceramics doped with Yb, Y, Nd, Ca and Li to the same general molecular formulation was studied at 1000°–1300°C in dry oxygen. Oxidation resistance of α-SiAlON ceramics increased in order of Li, Ca, Nd, Y, and Yb dopants. Oxide layers grown on Nd-, Y-, and Yb-doped samples were dense and crack-free whereas those formed on Ca- and Li-doped samples were porous. The dopant-dependent oxidation behavior of α-SiAlON ceramics can be attributed to the effect of the dopants on refractoriness of grain boundary phases and oxide layers as well as to the associated changes in the rate of grain boundary diffusion of dopants and oxygen diffusion in the oxide layers.

1. Introduction

SiAlON ceramics, the solid solutions of Si_3N_4 with oxygen, aluminum, and other select metal dopants, continue to attract considerable attention in both the research as well as the user community due to their excellent mechanical properties and thermal stability at high temperatures [1–7]. They are easier to sinter relative to Si_3N_4, thus rendering them significant cost advantage. Recent advance in making intrinsically hard α-SiAlON ceramics with whisker-like or elongated grain microstructures has led to the development of highly promising α-SiAlON ceramics with combined hardness, strength and fracture toughness [8]. The race is on to further improve the microstructure and grain boundary crystallinity of α-SiAlON ceramics, all of which will drive and accelerate their practical utilization in applications such as aircraft bearings, cutting tools, and turbine engine components [8, 9].

Silicon-based ceramics, e.g., SiAlON, Si_3N_4, and SiC, all share a common problem of oxidation degradation at high temperatures due to their thermodynamic instability in an oxidizing environment. A large body of literature exists on oxidation of Si_3N_4. While it is broadly recognized that pure and dense Si_3N_4 exhibits oxidation resistance superior to all other silicon-based ceramics, the oxidation resistance of hot-pressed or reaction-sintered Si_3N_4 is not as robust and is a strong function of the type and the amount of additive and impurity cations [10]. Of particular interest are recent oxidation studies of Si_3N_4 surface-alloyed with aluminum by implantation [11–13]. It was reported that aluminum implantation significantly reduced outward diffusion of Mg cation from the bulk ceramic to the oxide layer during oxidation in dry O_2, thus enhancing the oxidation resistance of Si_3N_4 sintered with MgO [11]. Similarly, incorporation of aluminum in Si_3N_4 markedly suppressed the adverse effect of sodium on the oxidation resistance of Si_3N_4 in O_2 enriched with $NaNO_3$ [12, 13]. Oxidation behavior of Si_3N_4 containing additives, impurities, as well as alloying elements (e.g., Al) are clearly dictated by how these species alter the characteristics of the oxide layers as well as ceramic grain boundaries. Such alteration significantly changes the rate of transport of oxygen in the oxide layer and of additive/impurity cations in the grain boundaries.

Oxidation investigation of SiAlON ceramics has been sparse, compared to their Si_3N_4 counterparts. Several comprehensive studies, particularly those by Nygren's team of Sweden, have yielded significant insights into the oxidation behavior of SiAlONs [14–18]. This ceramic system, with a large variety of choice dopants such as Nd, Sm, Gd, Y, Er, Y, Ca, and Li is far more complex in composition, phase types and structure. The complexity of the oxidation process for SiAlON ceramics has been reflected in the earlier oxidation studies [15–18]. The rate of oxidation of α-SiAlON ceramics has been shown to vary by orders of magnitude due to vastly different dopants that these ceramics can accommodate [15, 16, 18]. For instance, doping with Nd, Sm, Y, and Yb led to increased oxidation resistance of α-SiAlON ceramics in the same dopant order [15]. In general, the more refractory the grain boundary phases and oxide layers are the better the oxidation resistance of α-SiAlON ceramics. This family of ceramics is not yet competitive compared with Si_3N_4 from high-temperature oxidation stability viewpoint due mainly to high concentration of additive species. This gap is narrowing with continued proactive control

and improvement of grain boundary chemical and phase characteristics of α-SiAlON ceramics. In addition, the abundance of aluminum in α-SiAlON and the aluminum benefit exhibited in oxidation of Si_3N_4 under harsh environmental conditions (such as in the presence of sodium) [12, 13] will probably make it a compelling alternative for select applications, particularly given its combined hardness, strength and toughness.

This work aims to directly compare the effects of dopants on oxidation behavior of several laboratory α-SiAlON ceramics doped with Yb, Y, Nd, Ca and Li to the same general formulation. A turbine grade Si_3N_4 ceramic was included in the investigation for comparison. The role of dopants in the distinct oxidation characteristics of the α-SiAlON ceramics will be discussed.

2. Experimental

The composition of α-SiAlON ceramics investigated in this study can be represented by the general formula: $M_{m/z}Si_{12-(m+n)}Al_{(m+n)}O_nN_{16-n}$, where M stands for Yb^{3+}, Y^{3+}, Nd^{3+}, Ca^{2+} and Li^{+} cations. Symbol (m,n) is set to be (1.5, 1.2) for all dopants, which is referred to as 1512 composition (i.e., Yb1512, Y1512, Nd1512, Ca1512 and Li1512) in this paper. α-SiAlON platelet samples were made by hot-uniaxial pressing at the University of Pennsylvania. Details of the fabrication process of these ceramics can be found elsewhere [3–5]. SN282, a turbine grade Si_3N_4 was provided by Kyocera Industrial Ceramics Corporation. It was fabricated by cold-isostatic pressing for increased green density and high-temperature reaction bonding with 5.35 wt% Lu_2O_3 as sintering aid for densification. Atomic absorption analysis of SN282 yielded the following impurity phases: Yb_2O_3 (0.058 wt%), Al_2O_3 (0.045 wt%), Na_2O (0.053 wt%), CaO (0.016 wt%), and MgO (0.002 wt%).

α-SiAlON and SN282 samples were tribochemically polished to a high degree of surface finish with a measured root mean square roughness of 10–20 nm [19]. The polished samples were ultrasonically cleaned in de-ionized water, acetone, and methanol to remove surface contaminants before oxidation. Oxidation experiments of the α-SiAlON and Si_3N_4 samples were done in 1 atm dry oxygen flowing at 190 SCCM at 1000°–1300°C using a horizontal quartz tube-furnace (CM Furnaces, Bloomfield, NJ). Oxidation durations were 8 and 24 h. For each experiment, a total of six samples (five α-SiAlONs with different dopants and one SN282) were inserted into the hot zone of the furnace in a high-purity alumina boat so as to allow oxidation evaluation of the various samples under the same experimental condition.

The oxide thickness was measured and the oxide morphology determined using a field-emission gun scanning electron microscope (SEM) (LEO 982, LEO Electron Microscopy, Inc., Thornwood, NY) equipped with an energy dispersive spectroscopy (EDS) attachment. The cross-sectional samples for thickness measurements were prepared by first sectioning samples followed by brief preferential etching of the oxide via immersing the cross-section in buffered NH_4F:HF (10:1) solution. All samples were sputter-coated with a thin Au-Pd coat to minimize charging during SEM analysis due to their insulating nature. The phase characteristics of the oxidized samples were studied using X-ray diffraction (XRD) (Siemens Diffractometer D5000, Bruker AXS, Inc., Madison, WI).

3. Results

Oxidation of α-SiAlON and SN282 ceramics, despite their initial mirror surface finish, led to significant surface roughness. Optical methods such as ellipsometry and interferometry are therefore not suited for thickness determination of the oxide layers. Cross-sectional SEM proved a direct and reliable measurement technique for the thickness of the oxide layers grown on α-SiAlON and SN282 ceramics in current investigation. Summarized in Fig. 1 are thicknesses of oxide layers formed on α-SiAlON and SN282 ceramics in oxygen at 1000°–1300°C for 8 and 24 h. Logarithmic scale is

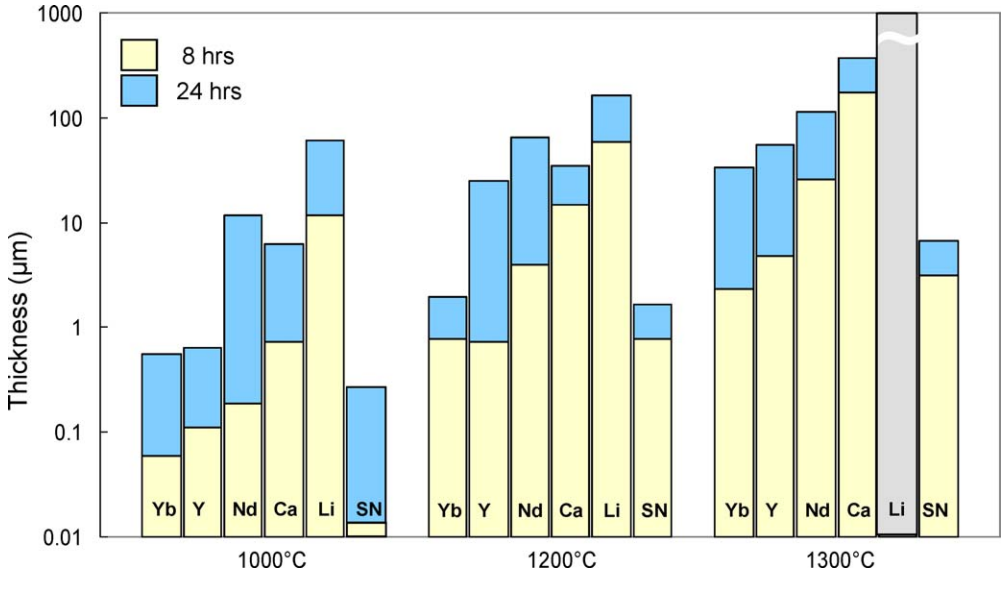

Figure 1 Thicknesses of oxide layers formed on α-SiAlON and SN282 ceramics in oxygen at 1000°–1300°C for 8 and 12 h.

TABLE I Crystalline phases in the oxidation layers grown on α-SiAlONs after oxidation in oxygen at 1000°–1300°C for 24 h

24 h	1000°C	1200°C	1300°C
Y-SiAlON	Cristobalite, Mullite	$Y_2Si_2O_7$, Cristobalite, Mullite	$Y_2Si_2O_7$, Cristobalite, Mullite
Yb-SiAlON	$Yb_2Si_2O_7$, Mullite, Cristobalite	$Yb_2Si_2O_7$, Mullite, Cristobalite	$Yb_2Si_2O_7$, Mullite, Cristobalite
Nd-SiAlON	$NdAlO_3$, Mullite, Cristobalite	$NdAlO_3$, Mullite, Cristobalite	$NdAlO_3$, Mullite, Cristobalite
Ca-SiAlON	$Ca_5Al_6O_{14}$, Mullite, Cristobalite	$Ca_5Al_6O_{14}$, Mullite, Cristobalite	$Ca_5Al_6O_{14}$, Mullite, Cristobalite
Li-SiAlON	$LiAlSi_3O_8$, Mullite, Cristobalite	$LiAlSi_3O_8$, Mullite, Cristobalite	$LiAlSi_3O_8$, Mullite, Cristobalite

used in order for inclusion of the results under all conditions. The thickness values were an average of five measurements with a typical variation of 5%. As shown in the figure, at 1000°C, the oxide layer grew to only about 0.06 μm thick on Yb1512 after oxidation for 8 h. In contrast, the oxide layer already reached a thickness of about 11.6 μm on Li1512 under the same oxidation condition. Oxidation resistance of α-SiAlON samples decreases in order of Yb, Y, Nd, Ca, and Li dopants. Oxidation of these ceramics intensified with increased temperature. In fact, spallation of the oxide layer occurred for Li1512 oxidized at 1300°C, resulting in inability to accurately determine the oxide thickness. The estimated thickness of oxide spalled off from Li1512 after 8 h of oxidation exceeds 1000 μm. The correlation between the oxidation resistance of α-SiAlON and the dopant type remains the same at each temperature. It is worth noting that SN282 exhibits the best oxidation resistance of all samples investigated.

Oxidation of α-SiAlON ceramics resulted in formation of crystalline silicates and aluminates of the constituent and dopant species. The crystalline phases in the oxidation layers formed on the α-SiAlONs, as identified by XRD, are listed in Table I. Common for all is the formation of cristobalite and mullite. The distinguishing feature in oxide phase characteristics amongst the various α-SiAlON ceramics is the presence of dopant-containing crystalline oxides, either silicates or aluminates. Illustrated in Figs 2 and 3, for example, are respective XRD patterns from Yb1512 and Li1512, two extreme samples from oxidation stability standpoint, after oxidation in oxygen at different temperatures for 24 h. Cristoballite and mullite are present in the oxides formed on both samples oxidized at 1000°–1300°C for Yb1512 and 1000°–1200°C for Li1512. Crystalline $Yb_2Si_2O_7$ is detected on Yb1512 and $LiAlSi_3O_8$ on Li1512. While diffraction intensity does not yield quantitative measure for different phases in a relative sense without further data treatment, it appears though that $LiAlSi_3O_8$ is the predominant crystalline oxide, compared to cristoballite and mullite, on Li1512. Cristoballite dominates the crystalline oxides on Yb1512. For Y1512, Nd1512, and Ca1512 oxidized under current conditions, in addition to cristobalite and mullite, $Y_2Si_2O_7$, $NdAlO_3$, and $Ca_5Al_6O_{14}$ are formed, respectively. In contrast, cristobalite and $Lu_2Si_2O_7$ are the main crystalline phases formed on oxidation-resistant SN282 silicon nitride under the same conditions.

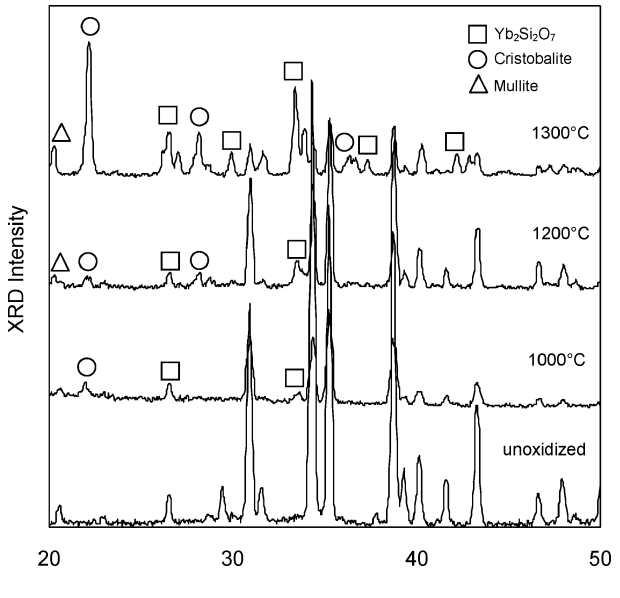

Figure 2 XRD pattern of Yb1512 after oxidation in oxygen at 1000°–1300°C for 24 h.

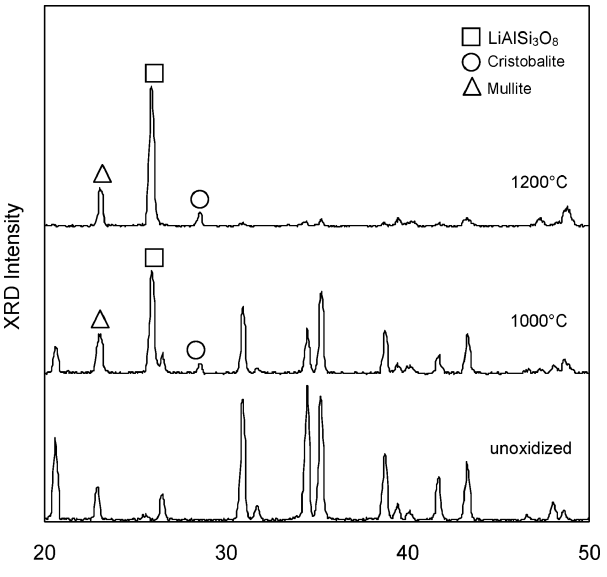

Figure 3 XRD pattern of Li1512 after oxidation in oxygen at 1000°–1200°C for 24 h.

Shown in Figs 4 and 5 are respective SEM micrographs of Yb1512, Y1512, Nd1512, Ca1512, and Li1512 samples after oxidation at 1200°C for 8 h. Corresponding cross-sectional SEM micrographs are also included for further morphological details across the thickness of the oxide layer. Common amongst Yb1512, Y1512, and Nd1612 samples is the emergence and growth of dopant-containing silicates ($Yb_2Si_2O_7$ or $Y_2Si_2O_7$) or aluminates ($NdAlO_3$) in the surface region of the oxidized samples (morphological features of light contrast), based on combined XRD and EDS analysis. According to Fig. 4a, the $Yb_2Si_2O_7$ phase exhibits a dendrite-like microstructure upon oxidation of

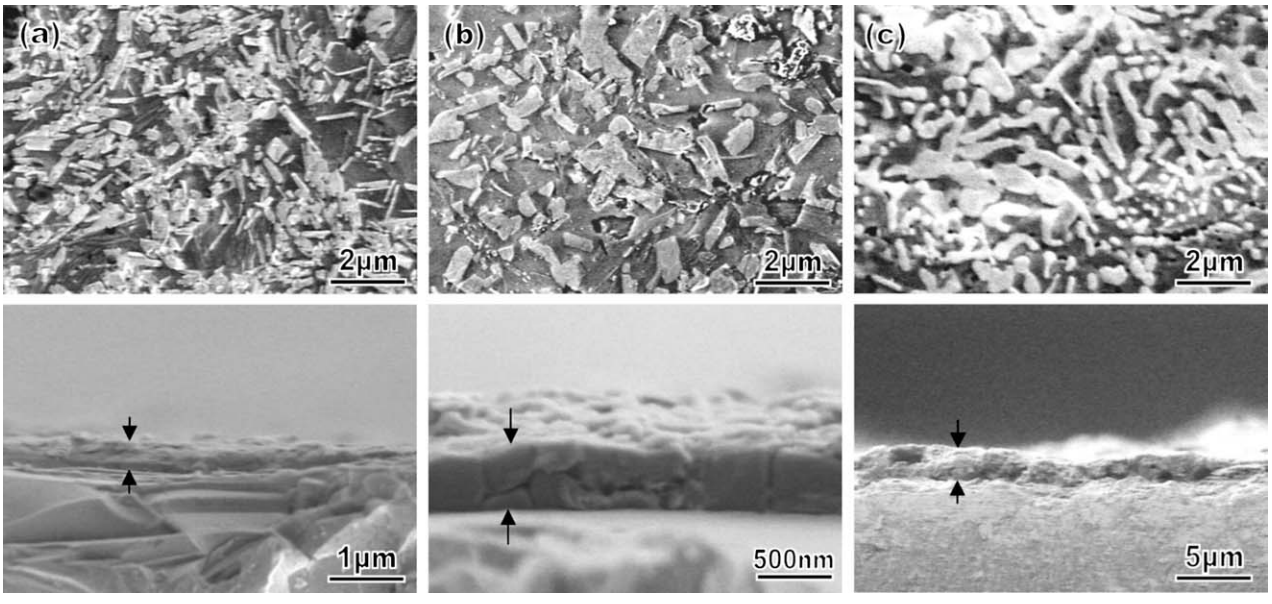

Figure 4 SEM plan view (top) and cross-sectional micrograph (bottom) of Y1512, Yb1512, and Nd1512 after oxidation at 1200°C for 8 h.

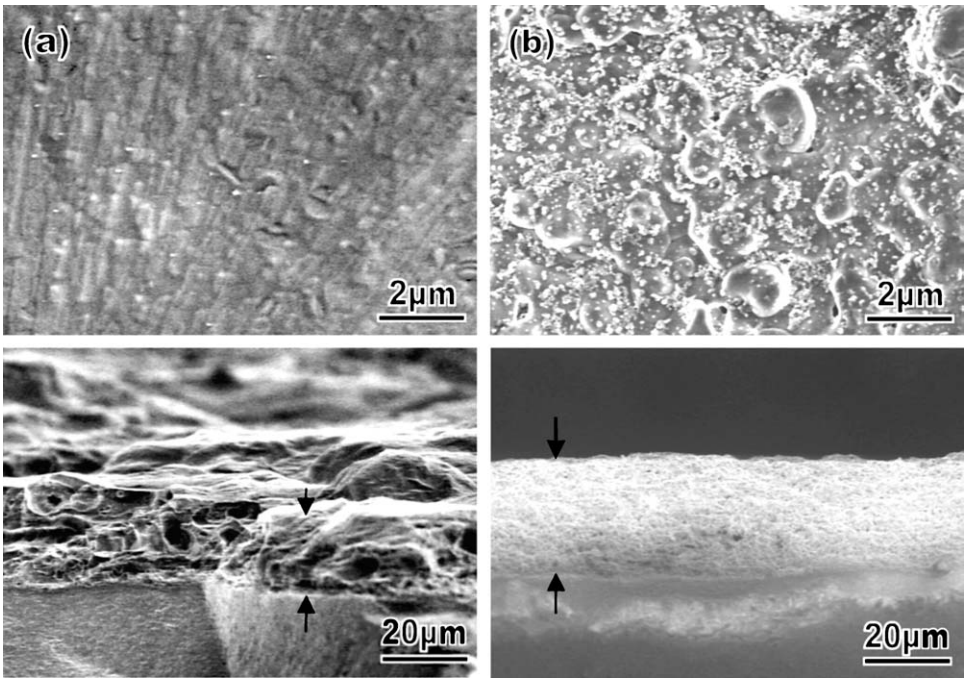

Figure 5 SEM plan view (top) and cross-sectional micrograph (bottom) of Ca1512 and Li1512 after oxidation at 1200°C for 8 h.

Yb1512 at 1000°C. The grains coarsened as oxidation temperature increased, leading to a dense grain structure at 1300°C. As seen in Fig. 4b, $Y_2Si_2O_7$ formed on Y1512 is of particulate appearance at 1000°C. Grain growth took place with increased temperature. Following Fig. 4c, $NdAlO_3$ grains on Nd1512 are needle-shaped of similar diameters at 1000°C. The grains coarsened significantly at 1200°C. The Nd1512 sample oxidized at 1300°C exhibits a morphological appearance of immersion of reticular $NdAlO_3$ grains in a molten oxide layer. The oxide layers grown on Yb1512, Y1512, and Nd1512 are dense.

The morphology of Ca1512 and Li1512 samples upon oxidation is not dominated by the formation of dopant-containing crystalline aluminates or silicates, as in the case of Yb1512, Y1512, and Nd1512, according to Fig. 5. In fact, the oxide layers are morphologically uniform. Cross-sectional SEM micrographs of Ca1512 oxidized at 1200°C revealed the porous nature of the oxide layers. Oxide layers formed on Li1512 are porous at 1100°–1300°C. Severity of oxide spallation was such that no intact region of the oxide layer could be found on Li1512 after oxidation at 1300°C.

4. Discussion

Oxidation resistance of α-SiAlON samples is strongly affected by the dopant type as shown in this work. While Yb1512 may have the potential to rival SN282, a turbine grade ceramic, in terms of oxidation stability, Li1512 exhibits inferior oxidation characteristics in the

temperature range investigated. The dopant type holds the key to the nature of the grain boundary phases and the oxide layer thus the oxidation behavior. Oxidation of α-SiAlON accelerated in order of Yb, Y, Nd, Ca, and Li dopants, which was also accompanied with an increased amount of dopant-containing silicate or aluminate in the oxide layer. This trend is a strong indication of the varying extent of dopant outward diffusion through grain boundaries of the ceramic bulk to the oxide layer and the subsequent formation of dopant-containing silicates or aluminates of vastly different refractory properties.

Ionic field strength, defined as the ratio of valence to radius square of a cation, is a useful unifying parameter to interpret the dopant-dependent oxidation process. It is a measurement of the bonding interaction of the cation with neighbor ions. Higher the field strength, the stronger the interaction is. Materials generally exhibit improved thermal and mechanical properties with increased ionic field strength [20]. Similar correlation exists in the processes and properties relevant to the current study, such as cation diffusivity, phase stability, and melting point and viscosity of the constituent silicates and aluminates. As the field strength increases, cation diffusivity decreases, stability and refractoriness of the silicates and aluminates increases, thus favoring enhanced oxidation stability. The respective ionic radii of Yb^{3+}, Y^{3+}, Nd^{3+}, Ca^{2+}, and Li^{+} are 0.86, 0.89, 1.0, 1.0 and 0.74 Å [21], yielding respective field strength of 4.05, 3.79, 3.00, 2.00, and 1.83 $1/Å^2$. This trend is consistent with that of the oxidation resistance of the corresponding α-SiAlON ceramics. The fact that rare-earth aluminosilicate glasses show increasing glass transition and softening temperatures as well as viscosity with decreasing radius of the rare earth cation [15, 22] lends significant support to field strength as a distinguishing factor.

Take Yb1512 and Li1512 as examples. The field strength of Yb^{3+} is significantly higher than that of Li^{+}. According to Figs 2 and 3, crystalline $LiAlSi_3O_8$ has a far higher diffraction intensity than cristobalite or mullite in the oxide layer on Li1512, compared with the diffraction intensity of $Yb_2Si_2O_7$ relative to cristobalite or mullite in the oxide layer on Yb1512. It can be stated that Li-enrichment in the oxide layer on Li1512 is far more prevalent than Yb-enrichment in the oxide layer on Yb1512. This sharp contrast is attributable to the rapid diffusion of Li^{+} from the underlying α-SiAlON ceramics to the oxide layer. No quantitative data are available for direct comparison between Yb^{3+} and Li^{+} for their diffusivity in a common material system. It is expected that the diffusivity of Yb^{3+} is orders of magnitude lower than that of Li^{+}.

Growth of an oxide layer consisting of cristoballite and mullite as common crystalline phases on α-SiAlON, regardless of the dopant type, results from the basic chemical nature of this ceramic family, i.e., a solid solution of Si_3N_4 with oxygen and aluminum, and as dictated by phase equilibrium of the SiO_2-Al_2O_3 system [21]. Cristoballite and mullite, when fully dense and free from microstructural defects such as cracks, are good diffusion barriers to oxygen thus form a protective layer on α-SiAlON. The inevitable formation of dopant-containing silicates and aluminates alters the chemical, phase, protective nature of the oxide layer and ultimately the oxidation resistance of α-SiAlON, evident in the current investigation.

Formation and growth of dopant-containing silicates and aluminates tends to take place in the surface region of the oxide layers for α-SiAlON doped with trivalent cations (i.e., Yb, Y, and Nd) (Fig. 4), as seen in other studies [16]. The crystalline features of the $Yb_2Si_2O_7$ and $Y_2Si_2O_7$ grains for samples oxidized at 1300°C are indicative of the refractory nature of these silicates. Embedment of reticular $NdAlO_3$ grains in a melt-like oxide layer for Nd1512 oxidized at 1300°C suggests the formation of a molten oxide layer during oxidation. The oxide layers on Yb1512, Y1512, and Nd1512 are dense with no apparent microstructural flaws. The significantly higher rate of oxidation of Nd1512 at 1200°–1300°C, compared with Yb1512 and Y1512, can be attributed to liquid phase formation in the oxide layer and perhaps the grain boundary phases. Liquid phase significantly facilitates inward oxygen diffusion in the oxide layer and outward dopant diffusion through grain boundary phases. The trivalent dopant-dependent oxidation behavior of α-SiAlON in this study is in agreement with earlier studies [15, 17], which reported decreased oxidation resistance of α-SiAlON in order of Yb, Y, and Nd dopants.

Alkali and alkaline earth species are glass modifiers and flux agents from glass formation point of view. They play a particularly detrimental role in oxidation resistance of silicon-based ceramics due to their fast diffusion nature and formation of oxides of low eutectic point and low melt viscosity. Ca1512 and Li1512 are no exception. Secondary phases in the grain boundaries of these ceramics are likely abundant and molten at the oxidation temperatures, resulting in rapid outward diffusion of dopants and formation of low eutectic phases in the oxide layer. Oxide layers are porous on Ca1512 (Fig. 5) and are of foam-like structure on Li1512. Bubble formation in the oxide layers is a classical indication of the evolution of nitrogen gas product through a low viscosity liquid oxide layer. The liquid nature of the oxide layers on Ca1512 and Li1512 samples allows rapid supply of oxygen from the environment to the oxide-SiAlON interface, leading to fast rate of oxidation and massive oxide spallation in the case of Li1512 during sample cooling.

It has been reported that dopant segregation to the oxide layer during oxidation may result in changes in local composition of SiAlON ceramics, thus α to β phase transformation [17]. β-SiAlON is known to exhibit poorer oxidation resistance than α-SiAlON [9, 15–17], due probably to higher secondary phases in grain boundaries. While our XRD analysis did not yield evidence of formation of β-SiAlON under current condition, α to β phase transformation can not be entirely ruled out, particularly for the Ca1512 and Li1512 samples where significant compositional changes and thus phase instability of α-SiAlON in the vicinity of the oxide-substrate interface may occur.

5. Conclusions

(1) α-SiAlON ceramics exhibit a strong, dopant dependent oxidation behavior. The oxidation resistance increases in order of Li, Ca, Nd, Y, and Yb.

(2) Silicates or aluminates of trivalent dopants (Yb, Y, and Nd) are formed as discrete refractory grains in the surface region of the oxide layers on α-SiAlONs. The oxide layers are dense and crack-free.

(3) No discrete silicates or aluminates grains of divalent (Ca) or monovalent (Li) dopants are found in the surface region of the oxide layers. The oxide layers are porous in nature with severe spallation in the case of Li1512.

(4) The refractory and dense nature of oxides on Yb-, Y-, and, to some extend, Nd-doped α-SiAlONs and the molten and porous state of the oxides on Ca- and Li-doped α-SiAlONs correspond well with the relative oxidation stability of the various α-SiAlONs ceramics.

(5) The dopant-dependent oxidation behavior can be explained based on the field strength of dopant cations, which decreases in order of Yb^{3+}, Y^{3+}, Nd^{3+}, Ca^{2+}, and Li^{+}. This correlation is consistent with the oxidation resistance and oxide morphology of the α-SiAlON ceramics investigated in the current study.

Acknowledgments

Work at the University of Pennsylvania is supported by the Air Force Office of Scientific Research under Grant No. AFOSR-G-F49620-01-1-0150. JY acknowledges the graduate assistantship support from Stevens Institute of Technology.

References

1. I.-W. CHEN and A. ROSENFLANZ, *Nature* **389** (1997) 701.
2. J. KIM, A. ROSENFLANZ and I.-W. CHEN, *J. Amer. Ceram. Soc.* **83** (2000) 1819.
3. M. ZENOTCHKINE, R. SHUBA, J. KIM and I.-W. CHEN, *ibid.* **85** (2002) 1254.
4. R. SHUBA and I.-W. CHEN, *ibid.* **85**, (2002) 1260.
5. M. ZENOTCHKINE, R. SHUBA and I.-W. CHEN, *ibid.* **85** (2002) 1882.
6. A. ROSENFLANZ and I.-W. CHEN, *ibid.* **82** (1999) 1025.
7. Z. B. YU, D. P. THOMPSON and A. R. BHATTI, *J. Eur. Ceram. Soc.* **20** (2000) 1815.
8. A. PECHENICK and I.-W. CHEN, *Adv. Mat. Proc.* March (2001) 37.
9. T. EKSTRÖM and M. NYGREN, *J. Amer. Ceram. Soc.* **75** (1992) 259.
10. N. S. JACOBSON, *ibid.* **76** (1993) 3.
11. P. MUKUNDHAN, H. DU and S. P. WITHROW, *ibid.* **85** (2002) 865.
12. Y. S. CHEONG, P. MUKUNDHAN, H. DU and S. P. WITHROW, *ibid.* **83** (2000) 154.
13. *Idem.*, *ibid.* **83** (2000) 159.
14. Anatoly Rosenflanz, *ibid.* **85** (2002) 2379.
15. L.-O. NORDBERG, M. NYGREN, P.-O. KÄLL and Z. SHEN, *ibid.* **81** (1998) 1461.
16. X. JIANG, Y.-K. BAEK, S.-M. LEE and S. L. KANG, *ibid.* **81** (1998) 1907.
17. Z. SHEN, P.-O. KÄLL and M. NYGREN, *Key Eng. Mat.* **132–136** (1997) 1576.
18. S. NAKAYAMA, A. SHIRANITA, N. AYUZAWA and M. SAKAMOTO, *J. Ceram. Soc. Jap.* **101** (1993) 1152.
19. S. R. HAN and T. R. FISCHER, *J. Electro. Soc.* **145** (1998) 1708.
20. PAUL F. BECHER, SHIRLEY B. WATERS, C. GRAY WESTMORELAND and LAURA RIESTER, *J. Amer. Ceram. Soc.* **85** (2002) 987.
21. W. D. KINGERY, H. K. BOWEN and D. R. UHLMANN, "Introduction to Ceramics," 2nd ed. (Wiley, New York 1976).
22. J. E. SHELBY and J. T. KOHLI, *J. Amer. Ceram. Soc.* **73** (1990) 39.

Received 19 June 2003
and accepted 6 May 2004